JOURNAL OF CELLULAR PHYSIOLOGY 208:527–537 (2006)

Multiple Apoptotic Pathways Induced by p53-Dependent Acidification in Benzo[a]pyrene-Exposed Hepatic F258 Cells

LAURENCE HUC,[1] MARY RISSEL,[1] ANITA SOLHAUG,[2] XAVIER TEKPLI,[1] MORGANE GORRIA,[1] ALICIA TORRIGLIA,[3] JØRN A. HOLME,[2] MARIE-THÉRÈSE DIMANCHE-BOITREL,[1] AND DOMINIQUE LAGADIC-GOSSMANN[1]*

[1]*Inserm U620, Université Rennes 1, IFR 140, Rennes, France*
[2]*Division of Environmental Medicine, Norwegian Institute of Public Health, Oslo, Norway*
[3]*Inserm U598, Institut Biomedical des Cordeliers, Paris, France*

Polycyclic aromatic hydrocarbons (PAH), such as benzo[a]pyrene (B[a]P), are ubiquitous genotoxic environmental pollutants. Their DNA-damaging effects lead to apoptosis induction, through similar pathways to those identified after exposure to other DNA-damaging stimuli with activation of p53-related genes and the involvement of the intrinsic apoptotic pathway. However, at a low concentration of B[a]P (50 nM), our previous results pointed to the involvement of intracellular pH (pH_i) variations during B[a]P-induced apoptosis in a rat liver epithelial cell line (F258). In the present work, we identified the mitochondrial F0F1-ATPase activity reversal as possibly responsible for pH_i decrease. This acidification not only promoted executive caspase activation, but also activated leucocyte elastase inhibitor/leucocyte-derived DNase II (LEI/L-DNase II) pathway. p53 appeared to regulate mitochondria homeostasis, by initiating F0F1-ATPase reversal and endonuclease G (Endo G) release. In conclusion, a low dose of B[a]P induced apoptosis by recruiting a large panel of executioners apparently depending on p53 phosphorylation and, for some of them, on acidification. J. Cell. Physiol. 208: 527–537, 2006. © 2006 Wiley-Liss, Inc.

Polycyclic aromatic hydrocarbons (PAH), such as benzo[a]pyrene (B[a]P), are formed during incomplete combustion of organic materials such as fossil fuels, coal, oil, and cigarettes, and found to be major environmental pollutants (Bostrom et al., 2002; Pfeifer et al., 2002).

Most of the biological effects of B[a]P are attributed to its biotransformation by xenobiotic-metabolizing enzymes, including CYP1A1 and 1B1. Some of the generated products are electrophilic, reactive, bind covalently to DNA and may thereby cause mutations and cancer (Pelkonen and Nebert, 1982). Depending on cell type, exposure to B[a]P may, however, result in diverse phenotypic responses such as increased cell proliferation (Brody and Rudel, 2003), alterations of energy metabolism (Salazar et al., 2004) as well as necrotic and apoptotic cell death (Solhaug et al., 2004). Most of these effects require binding to the aryl hydrocarbon receptor, AhR, which thereby induce a number of PAH-responsive genes, including various drug-metabolizing enzymes (Dertinger et al., 2000; Nebert et al., 2004).

Many studies have reported that exposure to PAH often result in an increased phosphorylation and accumulation of the tumor suppressor protein p53, probably as a result of DNA adduct formation (Kwon et al., 2002; Solhaug et al., 2004). The induced apoptosis appears to be linked to the DNA-damaging effects of PAH (Sparfel et al., 2004). The resulting cell signaling is rather similar to that identified after exposure to other DNA-damaging stimuli such as UV (Norbury and Zhivotovsky, 2004), with induction, repression or translocation of p53-regulated proteins, such as Bax or Bcl-2. Several studies have thus demonstrated the involvement of the intrinsic apoptotic pathway (Chen et al., 2003; Solhaug et al., 2004), but works by Chin and coworkers (Chin et al., 1998) have also suggested an activation of the extrinsic apoptotic pathway. Interestingly, PAH compounds have also been reported to upregulate Bax expression independently of p53 but dependent on an AhR-PAH binding element on Bax promoter (Matikainen et al., 2001). Furthermore, PAH have been found to induce an apoptosis dependent on the arachidonate pathway (Tithof et al., 2002). Considering all these possible PAH-induced effects, it therefore seems important to elucidate any possible cross-talks between the "classical" apoptotic pathways, the AhR-specific apoptotic pathways and other parameters that may modify the apoptotic effects of PAH such as intracellular pH (pH_i) (Lagadic-Gossmann et al., 2004).

Our previous studies have dealt with the role of pH_i in PAH-induced apoptotic death in a rat liver epithelial cell line (F258). They have revealed the involvement of an Na^+/H^+ exchanger 1 (NHE1) activation responsible for an early alkalinization, followed by a susbsequent mitochondria-dependent cytosolic acidification that seems to promote the apoptotic process (Huc et al., 2004). In order to gain further insight into any possible links between the diverse PAH-evoked cell signaling pathways, the present work has focused on the

Contract grant sponsor: Institut National de la Santé et de la Recherche Médicale (INSERM); Contract grant sponsor: Ligue Nationale Contre le Cancer (The Morbihan, Côte d'Armor and Ille et Vilaine Committees); Contract grant sponsor: Programme AURORA (Egide); Contract grant sponsor: Région Bretagne.

*Correspondence to: Dominique Lagadic-Gossmann, Inserm U620, Faculté de Pharmacie, Université Rennes 1, 2 av Prof Leon Bernard, 35043 Rennes cedex, France.
E-mail: dominique.lagadic@rennes.inserm.fr

Received 21 November 2005; Accepted 10 April 2006

DOI: 10.1002/jcp.20686

mitochondria-related acidification phase and its possible relationship with p53, caspase activation, and pro-apoptotic caspase-independent processes. Our data suggest that B[a]P exposure results in a reverse activity of the mitochondrial F0F1-ATPase following a p53-dependent mechanism, leading to cytosolic acidification, which in turn favors both activation of executive caspases and recruitment of the pH_i-sensitive leucocyte elastase inhibitor/leucocyte-derived DNase II (LEI/L-DNase II). Whereas the cytochrome *c* did not appear to be involved in this B[a]P-induced apoptotic cascade, translocation of endonuclease G (Endo G) to the nucleus seems to mediate another caspase-independent and possibly p53-dependent DNA cleavage.

MATERIALS AND METHODS

Chemicals

Benzo[a]pyrene, α-naphtoflavone (α-NF), etoposide, oligomycin (Oligo), antimycin A (AA), RNase A, propidium iodide, bongkrekic acid (BgA), N-Acetyl-Asp-Glu-Val-Asp-al-CHO (DEVD-CHO), DEVD-AMC (Asp-Glu-Asp-7-amino-4-methylcoumarin), fluorescein isothiocyanate (FITC)-conjugated anti-mouse IgG, and tetrarhodamine isothiocyanate (TRITC)-conjugated anti-rabbit IgG were purchased from Sigma Chemicals Co. (St. Louis, MO). Cyclic–Pifithrin α (PFT), caspase 8 inhibitor Z-Ile-Glu(O-ME)-Thr-Asp(O-Me)fluoromethy lketone (IETD-fmk), caspase 9 inhibitor Z-Leu-Glu(O-ME)-His-Asp(O-Me) fluoromethyl ketone (LEHD-fmk), global caspase inhibitor N-Benzyloxycarbonyl-Val-Ala-Asp(O-Me) fluoromethyl ketone (z-VAD), and cathepsin B inhibitor Z-Phe-Ala fluoromethyl ketone (FA-fmk) were purchased from Calbiochem (France Biochem, Meudon, France). All these products were used as stock solutions in dimethyl sulfoxide (Me_2SO), except for Oligo, which was dissolved in ethanol; final concentration of this vehicle in culture medium was <0.05% (v/v), and control cultures received the same concentration of vehicle as treated cultures. These products were used at concentrations which did not disturb CYP1-dependent metabolism of PAH. Hoechst 33342, mouse monoclonal anti-COX IV (clone 1D6) were purchased from Molecular Probes (Eugene, OR). Z-Asp-2, 6-dichlorobenzoyloxymethyl-ketone (Z-Asp) from Alexis Co. (Lausanne, Switzerland). Mouse monoclonal anti-apoptosis inducing factor (AIF), anti-HSC 70, anti-lamin A/C (346) and anti-β-actin, rabbit polyclonal anti-p53-phospho Serine 15, anti-Bax, anti-Mcl1 (S-19), and anti-caspase 3 antibodies were purchased from Santa Cruz Biotechnology (Tebubio SA, Le Perray en Yvelynes, France). Cariporide (caripo), an inhibitor of the Na^+/H^+ exchange isoform 1, was a kind gift from Aventis (Francfort, Germany). Mouse monoclonal anti-cytochrome *c* and anti-p53 antibodies were purchased from Pharmingen (San Diego, CA). Rabbit polyclonal anti-endoG antibody was kindly given by Dr. X. Wang (Southwestern Medical Center, Dallas, University of Texas). Rabbit polyclonal anti-LEI/L-DNase II antibody was prepared as previously described (Torriglia et al., 1998). Secondary antibody conjugated to horseradish peroxidase was from Dako A/S (Glostrup, Denmark).

Cell culture and apoptosis measurement

The F258 rat liver epithelial cell line was cultured in Williams' E medium supplemented with 10% fetal calf serum, 2 mM L-glutamine, 5 IU/ml penicillin, and 0.5 mg/ml streptomycin at 37°C under a 5% CO_2 atmosphere and treated 24 h following seeding as previously described (Payen et al., 2001; Huc et al., 2004). Microscopical detection of apoptosis was performed in both floating and adherent cells, using Hoechst 33342 labeling, as previously described (Huc et al., 2004). Caspase activity assay has been previously described (Gilot et al., 2002): caspase-mediated cleavage of DEVD-AMC was measured by spectrofluorimetry (Spectramax Gemini, Molecular Devices, Sunnyvale, CA) at the excitation/emission wavelength pair of 380/440 nm.

Transfection and RNA interference (siRNA)

Small interfering RNA (siRNA) oligonucleotide annealing was performed according to manufacturer's recommendations. siRNA oligonucleotides directed against p53 (si p53) (si p53 sens: 201059, sequence: NM_030989) and siRNA negative control duplex were, respectively, purchased from Ambion (Ambion Ltd., UK) and Eurogenetec (Eurogentec, Seraing, Belgium). siRNA Fluorescein (si Fluo) (Ambion Ltd.) was used to control transfection rate. Transfections of siRNA were performed in 60 mm dishes on 90% confluent F258 cells, in the presence of TransFectin Lipid Reagent (BioRad, Marnes la Coquette, France). Per dish, siRNA (100 nM) and 12.5 μl TransFectin lipid reagent were applied in a final volume of 2.5 ml Opti-MEM. Four hours later, the medium was renewed with the current medium as described above. The transfection rate was evaluated with si Fluo and corresponds to $87 \pm 4\%$ ($n = 4$) transfected cells. Cells were then passaged in order to be treated during exponential phase, as described above.

Measurement of pH_i

The pH_i of F258 cells cultured on glass coverslips was monitored using the pH-sensitive fluorescent probe, carboxy-SNARF-1 (carboxy-seminaphtorhodafluor; Molecular Probes), in Hepes-buffered solution, as previously described (Huc et al., 2004). The emission ratio 640/590 nm (corrected for background fluorescence) detected from intracellular SNARF was calculated and converted to a linear pH scale using in situ calibration obtained by the nigericin technique.

Western blotting immunoassays

After treatment, cells (both floating and adherent) were harvested, centrifuged, washed with PBS, and lysed for 20 min on ice in RIPA buffer (Lemarie et al., 2004). Then, DNA and cell debris were removed by centrifugation at 13,000 rpm for 15 min at 4°C. The resulting supernatants were collected and frozen at −80°C. Nuclear, cytosolic, and mitochondrial fractions were obtained as previously described (Poppe et al., 2001; Schneiderhan et al., 2003). Western blot analysis was performed as previously described (Joannard et al., 2006). Equal loading was checked by Ponceau technique, HSC 70, β-actin, COX IV, or lamin immunoblotting. Densitometry analysis of films was realized following each hybridization step.

Flow cytometry analysis of apoptosis (SubG1 population)

After treatment, cells, both adherent and floating, were harvested, centrifuged, washed with PBS. Cells were then fixed with PBS-ethanol 67% at 4°C during 30 min. After washing, cell nuclei were stained with propidium iodide (10 μg/ml) in presence of RNase A (10 μg/ml) during 1 h at 37°C. After washing, DNA content of 10,000 cells/analysis was monitored with a FACSCalibur cytometer (Becton Dickinson, BD Biosciences, San Jose, CA). Data were analyzed using Cell Quest software (Becton Dickinson) for peak detection of SubG1 hypoploid apoptotic cells. Three independent experiments were carried out.

Immunofluorescence assays

F258 cells were seeded into 35 mm dishes on glass coverslips and treated. After washing in PBS, adherent cells were fixed on coverslips with 4% paraformaldehyde in PBS for 30 min at 4°C and washed three times with PBS. Then, cells were incubated for 1 h with a blocking-permeabilizing solution (0.2% saponin-0.2% BSA in PBS). After washing, cells were incubated with either rabbit anti-phospho-p53, rabbit anti-endoG, rabbit anti-LEI/L-DNase II, mouse anti-AIF, or mouse anti-cytochrome *c* primary antibody in a blocking-permeabilizing solution for 2 h at room temperature, washed in PBS and then stained with TRITC-conjugated anti-rabbit IgG or FITC-conjugated anti-mouse IgG, respectively, for 1 h at room temperature. Thereafter, cells were co-stained by a 15 min incubation in a blocking solution containing 1 μg/ml DAPI, a fluorescent dye specific for DNA. After washing, coverslips were mounted with PBS-glycerol-Dabco. Fluorescent-labeled cells were captured with a DMRXA Leica microscope and a COHU high

performance CCD camera, using Metavue software. Data are representative of, at least, three independent experiments.

ATP determination

After treatment, ATP concentrations were measured using the CellTiter-Glo luminescent cell viability assay kit (Promega), following instructions provided by the manufacturer. Cells (2×10^4)/well were seeded into a 96-well plate. Half an hour before the end of treatment, cells were allowed to equilibrate to room temperature. The substrate was then added and the samples were read by luminometry (Spectramax Gemini, Molecular Devices).

Statistical analysis

All data are quoted as mean ± standard error of mean along with number of observations, n, corresponding, if not otherwise stated, to the number of separate cultures used. Analysis of variance followed by Newman–Keuls test was used to test the effects of B[a]P. Differences were considered significant at the level of $P < 0.05$.

RESULTS

B[a]P-induced acidification is related to p53 but independent of effector DEVD-like caspases

We have previously shown that B[a]P (50 nM) induced mitochondria-dependent acidification during apoptosis in F258 cells, after 72 h of treatment (Huc et al., 2004). In order to test the possible involvement of p53 in this effect, we first examined the activation of this tumor suppressor under our experimental conditions. In Figure 1A, Western blot analysis on total cell lysates indicated a dose-dependent increase of p53 phosphorylation on serine 15 (pp53) following a 20 h treatment with B[a]P. Immunolocalizations of pp53 in F258 cells treated with 50 nM B[a]P revealed a nuclear translocation at 48 and 72 h (Fig. 1B). Such a translocation was confirmed by Western blot analysis on isolated nuclear fraction (Fig. 1B) and was found to be inhibited by the transactivation inhibitor of p53, PFT (5 μM), as illustrated in Figure 1C. In order to block p53 activation more specifically, we also knocked down expression of p53 using the siRNA technology. Efficiency of p53 siRNA oligonucleotide (si p53) was monitored by immunolocalizations (Fig. 1D) and Western blots (Fig. 1E), in comparison with the negative siRNA oligonucleotide (si Neg). Immunolocalizations showed an inhibition of p53 phosphorylation and a blockage of its translocation (Fig. 1D) after a 48 h treatment with 5 μM of B[a]P. Moreover, the p53 level, detected in whole lysates from B[a]P-treated si Neg-transfected cells, was strongly diminished in B[a]P-treated, si p53-transfected cells (Fig. 1E).

Exploring a possible role for p53 in B[a]P-induced apoptosis in F258 cells, we performed both detection of hypoploid subG1 cells and Hoechst 33342 staining after a 72 h treatment, and found that PFT reduced apoptosis by 75% (Fig. 2A,B). Similarly, the si p53 transfection reduced the occurrence of apoptosis by about 69.4% ± 11.6 (n = 4), compared to the si Neg transfection (data not shown). Subsequently, we measured resting pH_i in F258 cells following a 72 h treatment with 50 nM B[a]P and 5 μM PFT in the presence of Hepes-buffered medium. Data illustrated in Figure 2C clearly show that B[a]P was not capable of inducing acidification under such conditions. Moreover, the measurement of resting pH_i in transfected cells showed that the p53 downregulation prevented B[a]P-induced acidification (Fig. 2D). Taken together, all these results suggested a role for p53 in triggering mitochondria-dependent acidification.

Likewise, we examined the involvement of effector caspases in both apoptosis and acidification. By using DEVD-CHO (5 μM) to inhibit caspase 3-like activities (data not shown), we found that while apoptosis was significantly reduced, by about 41% (Fig. 2A,B), the acidification was still maintained (Fig. 2C). Similar results were obtained with the global caspase inhibitor, Z-Asp (2 μM) (data not shown). Note that PFT, DEVD-CHO, and Z-Asp do not inhibit the early H_2O_2 formation and alkalinization (unpublished results).

Altogether, these results indicate that B[a]P induced apoptosis mainly through activation of the p53 pathway, which then triggered mitochondria-dependent cytosolic acidification, independently of caspase 3-like activities.

B[a]P-induced acidification may rely upon reverse activity of mitochondria F0F1-ATPase

The following set of experiments was performed with the aim of identifying the mitochondrial molecular actor of cytosolic acidification. We previously showed that BgA, which inhibits the adenine nucleotide translocator (ANT), prevented both acidification and apoptosis (Huc et al., 2004). In the present study, similar effects were observed with AA, which acts on the mitochondrial complex III (Fig. 3), thus pointing out the importance of the respiratory chain in these events. Previous works on apoptosis-related cytosolic acidification indicated a role for reverse activity of the mitochondrial ultimate electron transport chain complex (V, F0F1-ATPase) in this process, through extrusion of mitochondrial H^+ (Matsuyama et al., 2000). Such an activity might occur under our experimental conditions since B[a]P has recently been found to induce an hyperpolarization of mitochondrial membrane potential ($\Delta\Psi_m$) (Huc et al., 2003), a phenomenon suggested by others to be related to reversal of F0F1-ATPase activity (Khaled et al., 2001).

In order to test this hypothesis, we used Oligo (8 μM), an inhibitor of F0F1-ATPase, and measured resting pH_i following a 72 h co-treatment with 50 nM B[a]P. As illustrated in Figure 3, Oligo treatment prevented acidification (panel A) and was associated with a reduction of apoptosis by 60% (panels B–C). However, in order to test whether hydrolysis of intracellular ATP per se could be responsible for such an acidification, as previously suggested (Lang et al., 2000; Hirpara et al., 2001), we determined the ATP concentration following a 72 h B[a]P treatment. Figure 3D clearly illustrated that the different inhibitors (i.e., α-NF, an inhibitor of B[a]P metabolism; PFT; caripo, a specific NHE1 inhibitor; Oligo; and AA) differently affected the intracellular ATP level whereas they all prevented acidification (Figs. 2C and 3A in the present study; see also Huc et al., 2004 for caripo and α-NF). For example, PFT and AA prevented the ATP level decrease whereas Oligo and caripo did not, thus indicating that ATP drop was not directly responsible for acidification. Moreover, pyruvate-supplemented medium, which has been shown to maintain the ATP level, did not contribute to the survival of F258 cells following B[a]P treatment (unpublished data). Altogether, these results suggest that B[a]P-induced activation of the p53 pathway leads to F0F1-ATPase reversal, responsible for both cytosolic acidification and apoptosis.

Acidification could promote DEVD-like caspase activation

As shown in Figure 2C, DEVD-CHO had no effect on the induction of acidification, while partially protecting

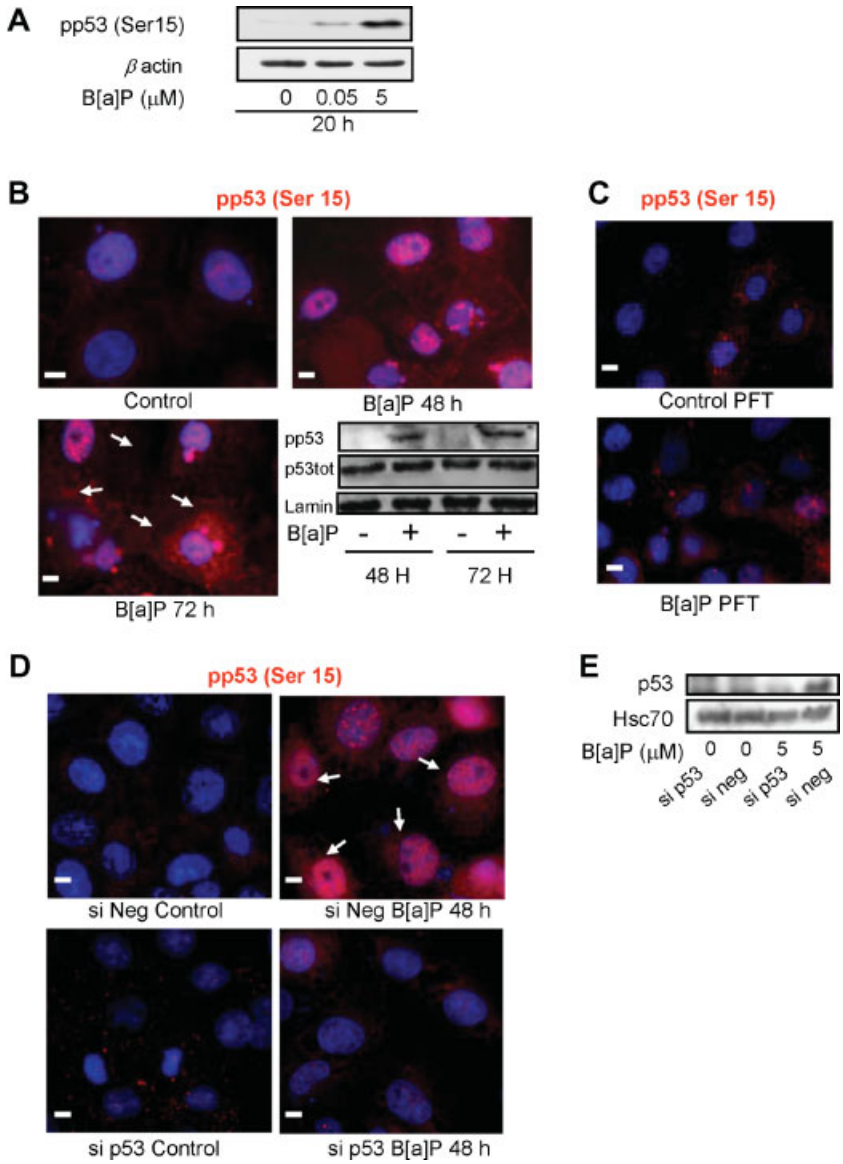

Fig. 1. Effects of B[a]P on p53 phosphorylation and nuclear translocation. **A**: F258 cells were treated with 0.05 or 5 μM B[a]P during 20 h. Whole cell lysate (60 μg) was separated on 12.5% SDS–polyacrylamide gel electrophoresis. Immunoblot was probed with a rabbit polyclonal anti-phospho-p53 (Ser 15) antibody and with a rabbit polyclonal anti-β-actin antibody as a loading control. Data are representative of three independent experiments. F258 cells were treated or not with 50 nM B[a]P during 48 and 72 h (**B**) or co-treated or not with 50 nM B[a]P and 5 μM PFT during 48 h (**C**). After fixation and permeabilization, immunostaining of cells was performed with a rabbit polyclonal anti-phospho-p53 (Ser15) antibody and with an anti-rabbit antibody, coupled to TRITC. Cells were co-stained with DAPI to detect nuclei and subsequently viewed by fluorescence microscopy (magnification 400×). Scale bar, 4 μm. Arrows indicate positive cells. Nuclear fractions (40 μg) (obtained as described in Materials and Methods) were separated on 12.5% SDS–polyacrylamide gel electrophoresis. Immunoblot was probed with a rabbit polyclonal anti-phospho-p53 (Ser 15) and mouse monoclonal anti-p53 and lamin antibodies. The experiments were repeated at least three times, with similar results. **D**: F258 cells were transfected with si Neg or si p53 and subsequently treated with 5 μM B[a]P during 48 h. After fixation and permeabilization, immunostaining of cells was performed with a rabbit polyclonal anti-phospho-p53 (Ser15) antibody and with an anti-rabbit antibody coupled to TRITC. Cells were co-stained with DAPI to detect nuclei and subsequently viewed by fluorescence microscopy (magnification 400×). The experiments were repeated at least three times, with similar results. Scale bar, 4 μm. Arrows indicate positive cells. **E**: Effect of si p53 on p53 expression in B[a]P (5 μM, 24 h)-treated F258 cells. Whole cell lysate (50 μg) was separated on 12.5% SDS–polyacrylamide gel electrophoresis. Immunoblot was probed with a mouse monoclonal anti-p53 antibody and with a mouse monoclonal anti-HSC 70 antibody as a loading control. Data are representative of three independent experiments.

cells from B[a]P-induced apoptosis. So, we finally investigated whether acidification was determinant for executioner caspase activation. Actually, some of our results were in favor of acidifying conditions playing a major role in DEVDase activity. First, in our model, no release of cytochrome *c* was observed upon 50 nM B[a]P treatment, whereas etoposide (10 μM) was able to induce such an event (Fig. 4A). Secondly, the use of the global caspase inhibitor Z-Asp (10 μM) did not protect more than the use of the specific inhibitor of executioner caspases DEVD-CHO (data not shown), and neither caspase 9 inhibitor (LEDH-fmk, 5 μM), nor caspase 8 inhibitor (IETD-fmk, 5 μM), used at low concentration in order to be isoform specific, prevented B[a]P-induced apoptosis (Fig. 4B), thus pointing to an activation of executioner caspases independently of initiator caspases. It is important to note that no caspase 8 and 9 activity was detected in this model (unpublished data).

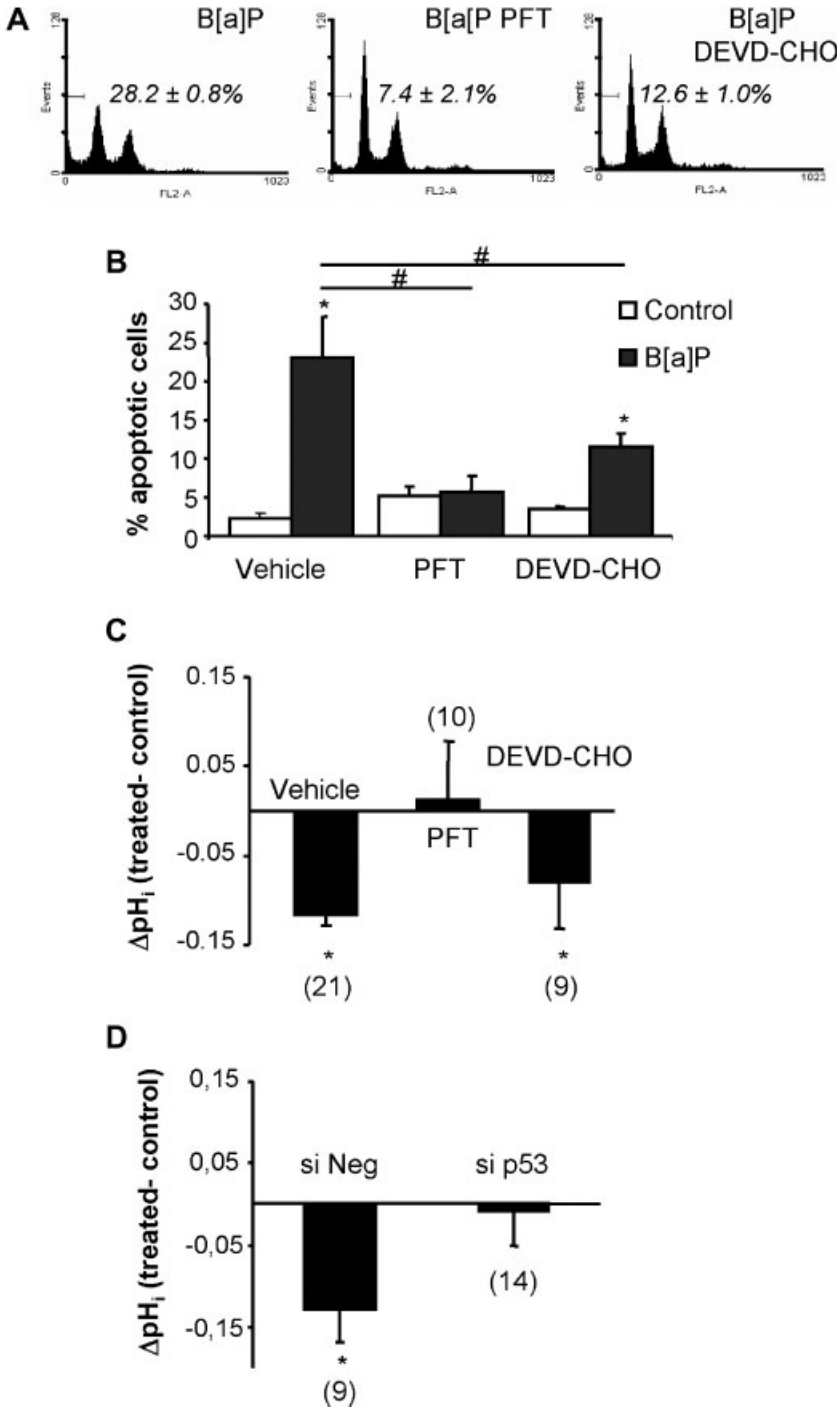

Fig. 2. Pifitrin α and p53 downregulation prevent both acidification and apoptosis, whereas DEVD-CHO only inhibits apoptosis upon B[a]P exposure. **A**–**C**: F258 cells were treated or not with 50 nM B[a]P and/or PFT (5 μM) or DEVD-CHO (5 μM) for 72 h. **D**: Cells were transfected with si Neg or si p53 and subsequently treated with 5 μM B[a]P during 48 h. A: Hypoploid subG1 cells (expressed in % ± standard error of total population) were then detected by flow cytometry following propidium iodide staining, as indicated in Materials and Methods. Histograms are representative of three independent experiments. B: Apoptotic nuclei were analyzed by Hoechst 33342 staining. *, $P < 0.05$, B[a]P versus control cells; #, $P < 0.05$, inhibitor and B[a]P-treated cells versus control B[a]P-treated cells (n = 4 independent experiments). C, D: Resting pH_i measurements were monitored by microspectrofluorimetry using the pH-sensitive fluorescent probe, carboxy-SNARF-1, in Hepes-buffered medium. pH_i values were derived from a pH calibration curve (as described in Materials and Methods) and ΔpH_i were calculated by subtracting pH_i values in untreated cells from those in treated cells. *, $P < 0.05$. Number in brackets given next to each bar represents the number of coverslips used (i.e., the number of performed measurements) from at least three independent experiments. Mean values correspond to the average of all pH_i determinations. Basal pH_i was 7.35 ± 0.02 (n = 21), 7.36 ± 0.03 (n = 10), 7.32 ± 0.06 (n = 9), in control untreated and PFT- or DEVD-CHO-treated cells, respectively. Basal pH_i was 7.34 ± 0.03 (n = 9) and 7.31 ± 0.02 (n = 14) in si Neg- and si p53-transfected untreated cells, respectively.

Thirdly, during the alkaline phase, detected after 48 h of treatment with 50 nM B[a]P (Huc et al., 2004), DEVDase activity was very weak, whereas, after a 72 h treatment, when pH_i was lower, DEVDase activity was increased by 2.5-fold. Moreover, at a higher concentration of B[a]P (5 μM), a larger acidification was induced as well as an enhanced DEVDase activity. As acidification has been previously reported to enhance autocatalytic activation

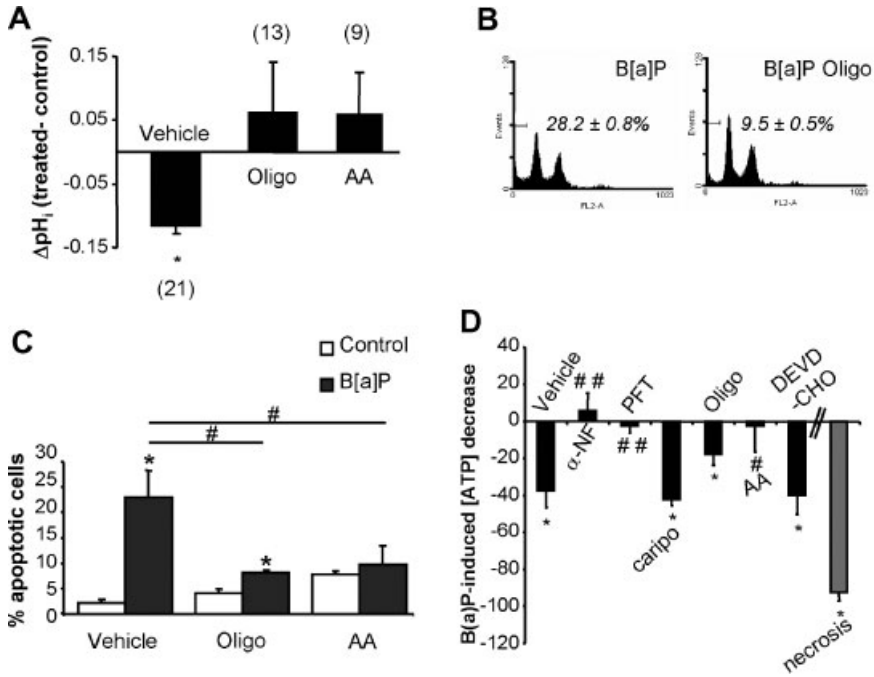

Fig. 3. Inhibitors of electron transport chain prevent B[a]P-induced acidification and apoptosis. **A**: F258 cells were treated with 50 nM B[a]P alone or in the presence of Oligo (8 μM) or AA (25 μM) during 72 h. ΔpH_i were calculated by subtracting pH_i values in untreated cells from those in treated cells. *, $P < 0.05$. Number in brackets given next to each bar represents the number of coverslips used (i.e., the number of performed measurements) from at least three independent experiments. Mean values correspond to the average of all pH_i determinations. Basal pH_i was 7.48 ± 0.09 (n = 13) and 7.40 ± 0.05 (n = 6) in control Oligo- and AA-treated cells, respectively. **B**: F258 cells were treated with 50 nM B[a]P alone or in the presence of Oligo (8 μM). Hypoploid subG1 cells (expressed in % ± standard error of total population) were then detected by flow cytometry following propidium iodide staining, as indicated in Materials and Methods. Histograms are representative of three independent experiments. **C**: F258 cells were treated with 50 nM B[a]P alone or in the presence of Oligo (8 μM) or AA (25 μM) during 72 h. Subsequently, apoptotic nuclei were analyzed by Hoechst 33342 staining. *, $P < 0.05$, B[a]P versus control cells; #, $P < 0.05$, inhibitor and B[a]P-treated cells versus control B[a]P-treated cells (n = 4 independent experiments). **D**: F258 cells were treated with 50 nM B[a]P alone or in the presence of α-NF (10 μM), PFT (5 μM), caripo (30 μM), Oligo (8 μM), DEVD-CHO (5 μM), and AA (25 μM) during 72 h in a 96-well plate. ATP content was evaluated as described in Materials and Methods. Values are obtained following an ATP standard curve and reported to the respective control. *, $P < 0.05$, B[a]P ± inhibitor versus control ± inhibitor cells. #, $P < 0.05$; ##, $P < 0.01$ inhibitor and B[a]P-treated cells versus control B[a]P-treated cells (n = 3 independent experiments).

of pro-caspases (Roy et al., 2001), we therefore decided to measure DEVDase activity in B[a]P-treated cells in the presence of inhibitors of acidification, that is, PFT, Oligo, and AA. As illustrated in Figure 4C, DEVDase activity was strongly inhibited by all these inhibitors. Moreover, when assessing the processing of pro-caspase 3 by Western blot, the occurrence of the cleaved form in B[a]P-treated cells was found to be prevented by co-treatment with α-NF, PFT, Oligo, or AA (Fig. 4D). Because Mcl1 has been previously described to be a potential target of acidification (Lagadic-Gossmann et al., 2004) and to be cleaved by caspase 3 (Weng et al., 2005), we analyzed its mitochondrial expression. In Figure 4E, Mcl1 was downregulated by B[a]P, but this event appeared to be only dependent on CYP metabolism and p53 (see α-NF and PFT). However, Mcl1 was also detected as the low-weight form at 27 kDa upon B[a]P treatment. The increase of this cleaved form ($Mcl1_C$) was strongly prevented by all the acidification inhibitors (α-NF, PFT, and Oligo), thus pointing to a relationship between the pro-apoptotic Mcl1 form appearance and the drop of pH_i. The use of DEVD-CHO, which inhibited caspase 3 activity, prevented the increase of $Mcl1_C$. Altogether, these results suggest an important role for acidification as a permissive factor in caspase 3 activation and consequently, in the appearance of the pro-apoptotic form $Mcl1_C$ during B[a]P-induced apoptosis.

B[a]P-induced Endo G release is possibly related to p53 activation but independent of acidification

In the following experiments, we decided to test the release from mitochondria of various pro-apoptotic proteins, notably those involved in caspase-independent pathways, because only a partial protection was afforded when inhibiting executioner caspases (Fig. 2C). Since no release of cytochrome *c* was detected upon B[a]P treatment (Fig. 4A), we next examined any possible involvement of AIF, which we have shown to be translocated from mitochondria to nucleus during cadmium-induced apoptosis (Lemarie et al., 2004); however, no apparent variation in the pattern of AIF immunoreactivity upon B[a]P exposure for 72 h was observed (data not shown). On the other hand, Endo G whose activation is also known to be caspase independent, was released from mitochondria and detected in apoptotic nuclei (Fig. 5A,B) and cytosol (Fig. 5C) following a 72 h exposure with B[a]P. The inhibition of CYP1-dependent metabolism by α-NF prevented such a release (data not shown). Whereas, in the presence of inhibitors of acidification, that is, BgA and Oligo, or inhibitors of DEVD-like activities, that is, DEVD-CHO or z-VAD, EndoG was still translocated into the nucleus, PFT prevented such an effect, suggesting the involvement of p53. In conclusion, B[a]P-induced Endo G release may be dependent on the formation of reactive

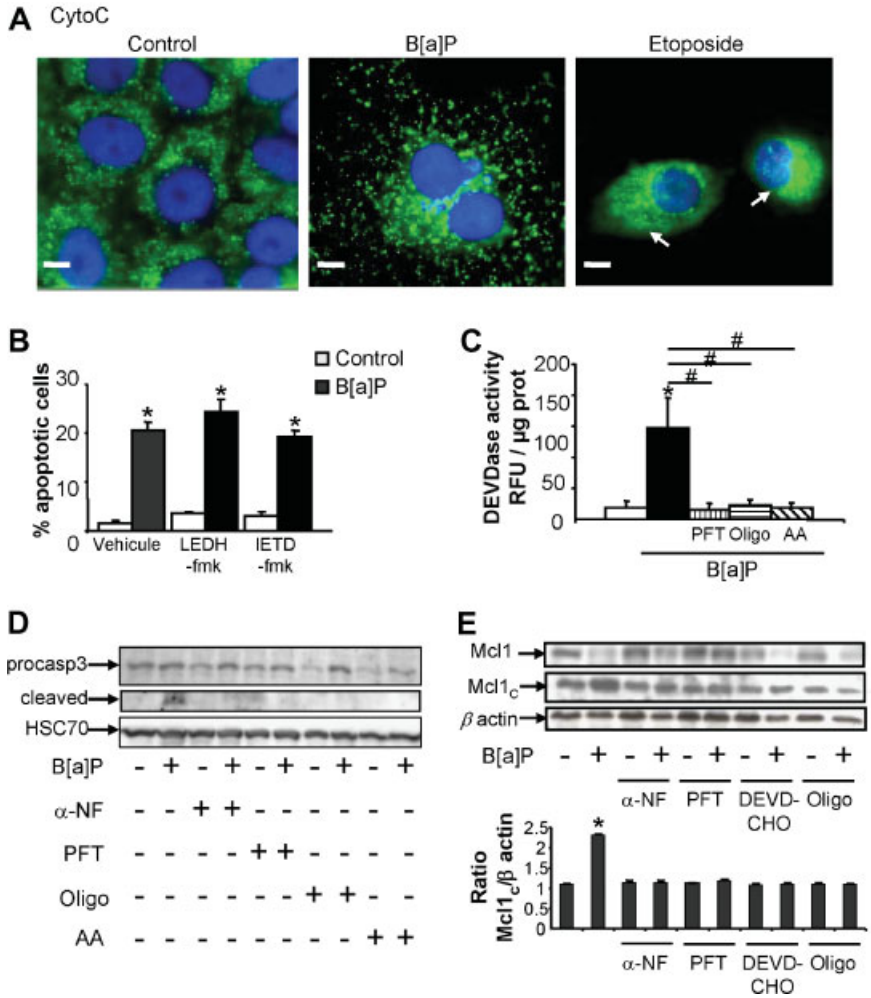

Fig. 4. Activation of caspase 3 is favored by B[a]P-induced acidification. **A**: F258 cells were treated or not with 50 nM B[a]P or 10 μM etoposide during 72 h. Etoposide was used as a control for cytochrome *c* release. After fixation and permeabilization, immunostaining of cells was performed with mouse monoclonal anti-cytochrome *c* antibody by using as secondary antibody an anti-mouse coupled to FITC. Cells were co-stained with DAPI to detect nuclei and subsequently viewed by fluorescence microscopy (magnification 650×). The experiments were repeated at least three times, with similar results. Scale bar, 4 μm. **B**: F258 cells were treated with 50 nM B[a]P alone or in the presence of LEDH-fmk (5 μM) or IETD-fmk (5 μM) during 72 h. Subsequently, apoptotic nuclei were analyzed by Hoechst 33342 staining. *, $P < 0.05$, B[a]P versus control. **C**: F258 cells were treated with 50 nM B[a]P alone or with PFT (5 μM), Oligo (8 μM), or AA (25 μM) during 72 h. DEVDase activities were measured by spectrofluorimetry, averaged from five independent experiments and expressed as RFU/μg proteins. *, $P < 0.05$, B[a]P ± inhibitor versus control ± inhibitor; #, $P < 0.05$, B[a]P + inhibitor versus B[a]P-treated cells. **D**: Western blot analysis of caspase 3. F258 cells were treated with 50 nM B[a]P alone or in the presence of α-NF (10 μM), PFT (5 μM), Oligo (8 μM), or AA (25 μM) during 72 h. Whole cell lysate (40 μg) was separated on 13% SDS–polyacrylamide gel electrophoresis. Immunoblot was probed with rabbit polyclonal anti-caspase 3 antibody and with mouse monoclonal anti-HSC 70 antibody as a loading control. Data are representative of four independent experiments. **E**: Western blot analysis of Mcl1. F258 cells were treated with 50 nM B[a]P alone or in the presence of α-NF (10 μM), PFT (5 μM), DEVD-CHO (5 μM), or Oligo (8 μM) during 72 h. Mitochondrial fractions (40 μg) (see Materials and Methods) were separated on 12% SDS–polyacrylamide gel electrophoresis. Immunoblot was probed with rabbit polyclonal anti-Mcl1 antibody and with mouse monoclonal anti-β-actin antibody as a loading control. Quantitative analysis of $Mcl1_c$ by densitometry is given in the histogram. The results are expressed as the ratio of $Mcl1_c$ to that of total β-actin. Data are representative of three independent experiments. *, $P < 0.05$, B[a]P versus control.

B[a]P metabolites and possibly p53 activation but apparently not on acidification.

Acidification triggers cathepsin B-mediated activation of LEI/L-Dnase II upon B[a]P exposure

After having examined the involvement of mitochondrial proteins, we next looked for pathways possibly sensitive to acidification. So, we focused on LEI/L-DNase II, an anti-protease that exhibits a DNase activity when cleaved following acidification in apoptotic cells (Altairac et al., 2003). In Figure 6A, the LEI was detected as a 42 kDa protein in total lysate of control cells. After development of acidification, the appearance of the 35 kDa band was visualized in B[a]P-treated cells at 96 h, showing that LEI/L-DNase II had lost its anti-elastase activity and gained its nuclease activity. By subcellular fractionation and by immunolocalization, we confirmed the activation and nuclear translocation of L-DNase II; indeed we detected the fully active 27 kDa form in nuclear fraction (absent in cytosolic fraction) by Western blot (Fig. 6B) and localized the protein in the fragmented nuclei of apoptotic cells following B[a]P treatment (Fig. 6C). The use of α-NF and PFT prevented the band shift (Fig. 6A,B).

In order to determine whether acidification was a necessary condition for the DNase II activation by B[a]P, we treated cells with both 50 nM of B[a]P and an inhibitor of acidification, that is, BgA (Huc et al., 2004); as shown in Figure 6C, B[a]P-induced translocation of LEI/L-DNase II in the nucleus was prevented by this

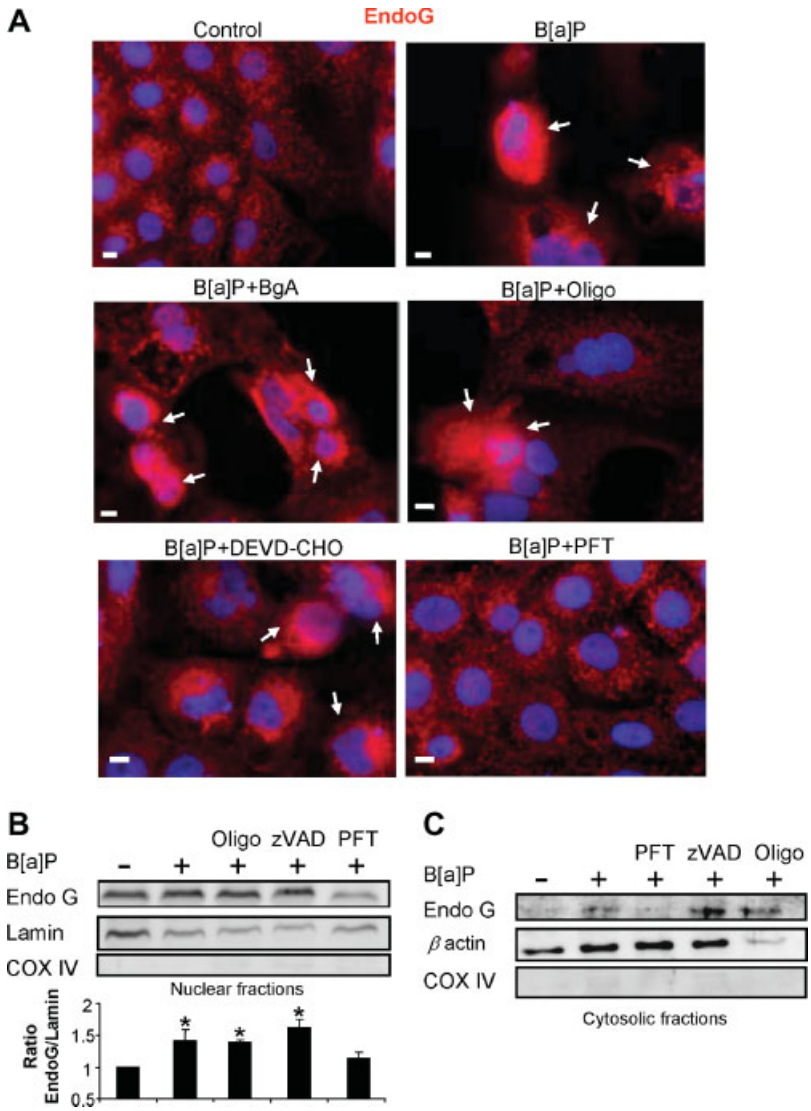

Fig. 5. Release of EndoG is independent of acidification but dependent on p53 activation. F258 cells were treated or not with 50 nM B[a]P during 72 h, in presence or not of BgA (10 μM), Oligo (8 μM), DEVD-CHO (5 μM), z-VAD (5 μM), or PFT (5 μM). **A**: After fixation and permeabilization, immunostaining of cells was performed with rabbit polyclonal anti-EndoG antibody, by using as secondary antibody an anti-rabbit coupled to TRITC. Cells were co-stained with DAPI to detect nuclei and subsequently viewed by fluorescence microscopy (magnification 400×). The experiments were repeated at least three times, with similar results. Scale bar, 4 μm. Arrows indicate positive cells. **B**: Western blot analysis of nuclear EndoG. Nuclear fractions (40 μg) (obtained as described in Materials and Methods) were separated on 12.5% SDS–polyacrylamide gel electrophoresis. Quantitative analysis of nuclear EndoG by densitometry is given in the histogram. The results are expressed as the ratio of EndoG to that of lamin. Data are representative of three independent experiments. *, $P < 0.05$, B[a]P versus control. **C**: Western blot analysis of cytosolic EndoG. Cytosolic fractions (40 μg) (obtained as described in Materials and Methods) were separated on 12.5% SDS–polyacrylamide gel electrophoresis. Immunoblot was probed with a rabbit polyclonal anti-EndoG antibody. The fraction purity was tested with antibodies directed against lamin and COX IV. The experiments were repeated at least three times, with similar results.

molecule. Moreover, as previous results suggested the involvement of cathepsins in acidification-mediated LEI/L-DNase II cleavage (Altairac et al., 2001), we tested a specific inhibitor of cathepsin B (FA-fmk, 1 μM). As shown in Figure 6B,C, LEI cleavage and DNase II translocation were prevented by this inhibitor. Moreover, when evaluating the protective effect of FA-fmk on B[a]P-induced apoptosis by Hoechst staining, we found a reduction by about 31% of the induced apoptosis (Control: 1.75 ± 0.01; B[a]P: 24.00 ± 0.04; Control + FA-fmk: 0.75 ± 0.01; B[a]P + FA-fmk: 16.50 ± 0.01% of apoptotic cells). Interestingly, no effect of FA-fmk was observed on DEVDase activity (data not shown). Thus, LEI/L-DNase II seemed to be a target for the acidification related to B[a]P-induced apoptosis, likely via cathepsin B involvement.

DISCUSSION

The present study has more thoroughly examined the role played by the mitochondria-dependent acidification phase, in relation with p53 induction and caspase activation, in B[a]P-treated hepatic cells. Here, we show for the first time that B[a]P triggers mitochondrial dysfunction likely through the induction of reverse activity of the mitochondrial H^+ pump F0F1-ATPase. This reversal seems to rely upon p53 activation, and would lead to cytosolic acidification, through proton extrusion from the mitochondrial matrix. This decrease of pH_i can then play a major role in both executive caspase activation and recruitment of the pH_i-sensitive LEI/L-DNase II, apparently without any involvement of either cytochrome *c* or AIF. However, a release of EndoG from

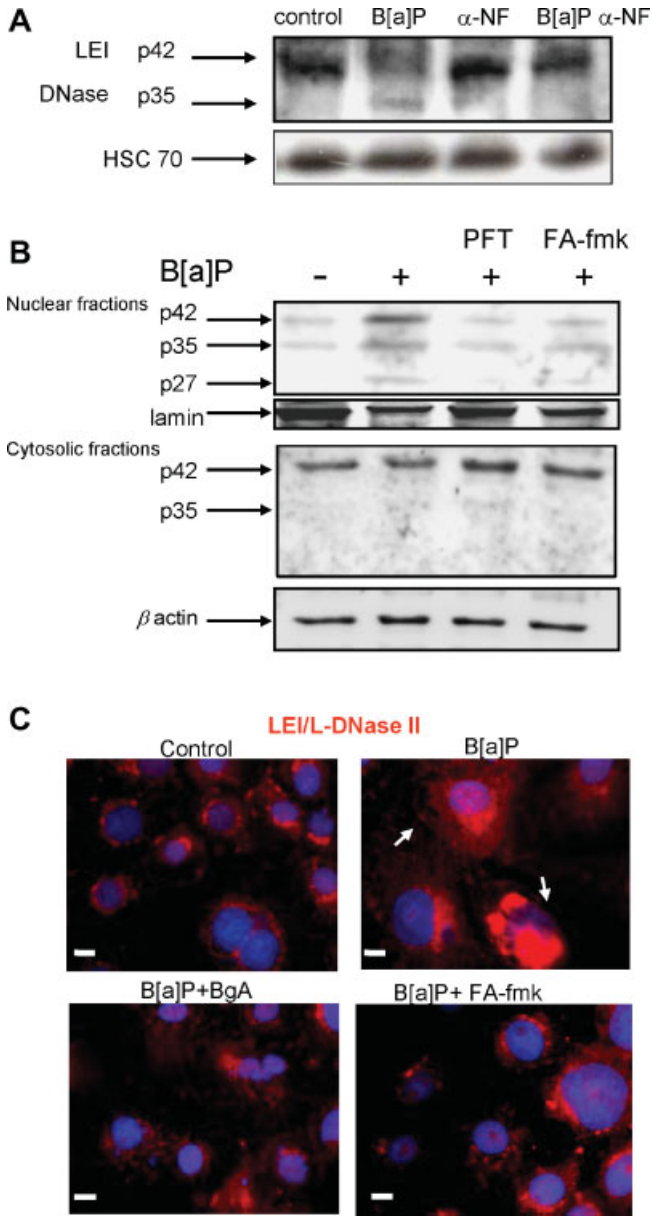

Fig. 6. Activation of LEI/L-DNase II during B[a]P-induced apoptosis. F258 cells were treated with 50 nM B[a]P alone during 96 h (**A**–**C**) or co-treated with (A) α-NF (10 μM), (B) PFT (8 μM), (B, C) FA-fmk (1 μM), (C) BgA (10 μM). A, B: Western blot analysis of LEI/L-DNase II. Whole cell lysate (40 μg) (A) or nuclear and cytosolic fractions (B) were separated on 12.5% SDS–polyacrylamide gel electrophoresis. Immunoblot was probed with rabbit polyclonal anti-LEI/L-DNase II antibody and with mouse monoclonal anti-HSC 70, anti lamin A/C, and anti-β-actin antibodies as loading controls for total lysate, nuclear and cytosolic fractions, respectively. Data are representative of three independent experiments. C: After fixation and permeabilization, immunostaining of cells was performed with a rabbit polyclonal anti-LEI/L-DNase II antibody and an anti-rabbit coupled to TRITC. Cells were co-stained with DAPI to detect nuclei and subsequently viewed by fluorescence microscopy (magnification 400×). The experiments were repeated at least three times, with similar results. Scale bar, 4 μm. Arrows indicate positive cells. The % of cells with nuclear LEI/L-DNase II expression in control, B[a]P, BgA, and BgA + B[a]P-treated cells were evaluated at 0.4 ± 0.1 (n = 4), 22.4 ± 0.5 (n = 4), 0.5 ± 0.1 (n = 3), and $4.4 \pm 0.5\%$ (n = 3), respectively.

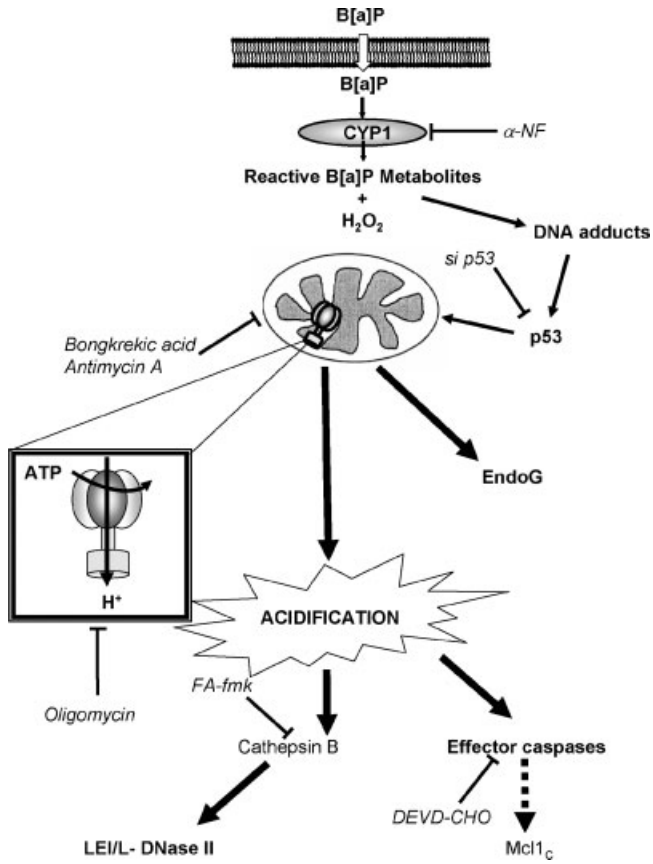

Fig. 7. Recapitulative model of the mechanisms involved in the acidification-dependent, B[a]P-induced apoptosis. B[a]P, a lipophilic molecule, goes across the bilayer membrane. In the cytosol, B[a]P is metabolized by CYP1 into reactive metabolites, which form DNA adducts, leading to p53 activation. This activation favors the apoptotic signaling via mitochondria, leading to a dysfunction of F0F1-ATPase. Reverse activity of the F0F1-ATPase, inhibited by Oligo and AA, would induce a cytosolic acidification, which would favor independent and dependent caspase pathways: activation of the pH_i-sensitive endonuclease LEI/L-DNase II via the cystein protease cathepsin B, and cleavage of caspase 3, which could lead to cleavage of the anti-apoptotic protein Mcl1. Moreover, B[a]P-induced apoptosis would also rely upon release of EndoG from mitochondria, also dependent on p53.

mitochondria, found to be dependent on the formation of reactive metabolites and p53 activation, would also be involved in B[a]P-induced apoptosis, though independently of intracellular acidification (Fig. 7).

Reverse activity of the mitochondrial F0F1-ATPase under apoptotic conditions was first described by Matsuyama and coworkers (Matsuyama et al., 1998, 2000; Matsuyama and Reed, 2000) but the underlying molecular mechanisms are still poorly understood. In the present study, acidification is clearly independent of caspase activation and inhibited by Oligo, as previously demonstrated (Matsuyama and Reed, 2000). However, its dependence on p53 pathway does not rely on Bax activation (unpublished data), in contrast to what was previously suggested (Matsuyama et al., 1998; Matsuyama and Reed, 2000).

In this context, how does p53 induce reverse F0F1-ATPase activity? Considering the recent work by Chipuk et al. (2005), a direct role of p53 on mitochondria could occur under our experimental conditions, coordinated by Bcl-xL and the pro-apoptotic BH3-only protein PUMA. In such a scheme, one might indeed propose that pp53 (Ser 15), localized in the nucleus, might upregulate the expression of PUMA (Nakano and Vousden, 2001; Yu et al., 2001), which would then trigger the release of the cytoplasmic p53 from Bcl-xL with consequent translocation to mitochondria in order to modulate the

F0F1-ATPase. As PFT and si p53 blocked the primary pp53 nuclear accumulation induced by B[a]P in our model, the secondary mitochondrial action of p53, if occurring, would consequently be prevented due to the absence of PUMA induction, thereby possibly underlying the inhibition of intracellular acidification by PFT and si p53. Considering the importance of PUMA in numerous apoptotic pathways, including DNA damage (Jeffers et al., 2003), its involvement in B[a]P-induced apoptosis will therefore have to be evaluated in the future.

In our model, acidification appears to play a crucial role in directing B[a]P toxicity towards apoptosis. Indeed, the present data have shown that this caspase-independent, mitochondria-mediated event favored the executive phase of apoptosis, via both caspase-dependent (caspase 3) and -independent (LEI/L-DNase II) pathways. Indeed, all these effects were inhibited by cell treatments that hampered acidification (i.e., PFT or BgA). Regarding the caspase pathway, our results would tend to favor the hypothesis that acidic conditions alone might allow removal of the pro-caspase 3 dormancy, as previously demonstrated by Roy et al. (2001). Application of low doses of nigericin (0.05–0.1 μM) after 60 h treatment, in order to equilibrate pH_i to extracellular pH during acidification phase, did not allow us to conclude about a potential direct role of acidification on caspase processing because of the loss of cellular integrity. Moreover, our results further reveal that these enzymes would exhibit only a partial role in B[a]P-induced apoptosis, since only 40% of apoptosis was prevented by DEVD-CHO and Z-Asp, thus suggesting a primordial role of caspase-independent pathways. Nonetheless, it is worth noting that, in our cell model, caspase activation triggered the cleavage of the anti-apoptotic protein Mcl1, which could act as a pro-apoptotic factor and participate in a positive feedback loop leading to further mitochondrial disturbance (Michels et al., 2005). Regarding LEI/L-DNase II cleavage and related endonuclease activity, we are the first to identify the involvement of such a protein during B[a]P-induced apoptosis. Its role in xenobiotic-induced apoptosis was previously demonstrated in pigmented epithelial cells after ethanol treatment (Brossas et al., 2004). Furthermore, from the results obtained with FA-fmk, it appears that LEI/L-DNase II activation upon acidification would rely on the cystein protease cathepsin B activation (Mort and Buttle, 1997).

Concerning the caspase-independent pathways elicited by B[a]P, our data showed that EndoG was translocated from mitochondria to nuclei, independently of acidification and AIF. EndoG might act either alone when massively translocated into nucleus, or following prior DNA digestion by L-DNase II. It is worth noting here that EndoG release and LEI/L-DNase II were previously described during light-induced photoreceptor apoptosis (Chahory et al., 2004; Wenzel et al., 2005), which might suggest that this cooperativity could exist. Our data also suggest that, in the absence of mitochondrial pore transition (Zamzami and Kroemer, 2001) and cytochrome *c* release, EndoG could be selectively released from the mitochondrial intermembrane space; in this context, a partial and selective external membrane permeabilization might be sufficient and Ca^{2+} homeostasis could regulate such event (Lemarie et al., 2004).

In our model using a low concentration of B[a]P, the induced DNA damage seems to be followed by several DNA replications and modifications of enzyme activities including ion transporters, before generating the ultimate triggering signal for apoptosis. Thus, whereas a higher B[a]P concentration, applied to cells which exhibit high CYP metabolism, would rapidly activate the pro-apoptotic machinery (Bax induction, Bcl-2 downregulation) (Matikainen et al., 2001; Norbury and Zhivotovsky, 2004) leading to a massive cell death following well-established pathways, a sort of "social dialogue" between nucleus, mitochondria, and other organelles might occur in case of a low concentration in order to determine cell fate (Knight and Petit, 2001); in this context, the activation of a large range of apoptotic executioner molecules (caspases, EndoG, LEI/L-DNase II), upon acidic conditions more permissive for such activities (Roy et al., 2001; Altairac et al., 2003; Schafer et al., 2004), rather than exclusively caspases, might reflect such a dialogue.

ACKNOWLEDGMENTS

We want to thank the microscopy platform and Dr. Dutertre (UMR 6061, CNRS, Rennes) for helpful advice on immunolocalization captures and analyses.

LITERATURE CITED

Altairac S, Chaudun E, Courtois Y, Torriglia A. 2001. Elastase is not required for L-DNase II activation during apoptosis in developing chicken neural retina. Neurosci Lett 303(1):41–44.

Altairac S, Zeggai S, Perani P, Courtois Y, Torriglia A. 2003. Apoptosis induced by Na^+/H^+ antiport inhibition activates the LEI/L-DNase II pathway. Cell Death Differ 10(5):548–557.

Bostrom CE, Gerde P, Hanberg A, Jernstrom B, Johansson C, Kyrklund T, Rannug A, Tornqvist M, Victorin K, Westerholm R. 2002. Cancer risk assessment, indicators, and guidelines for polycyclic aromatic hydrocarbons in the ambient air. Environ Health Perspect 110(Suppl 3):451–488.

Brody JG, Rudel RA. 2003. Environmental pollutants and breast cancer. Environ Health Perspect 111(8):1007–1019.

Brossas JY, Tanguy R, Brignole-Baudouin F, Courtois Y, Torriglia A, Treton J. 2004. L-DNase II associated with active process during ethanol induced cell death in ARPE-19. Mol Vis 10:65–73.

Chahory S, Padron L, Courtois Y, Torriglia A. 2004. The LEI/L-DNase II pathway is activated in light-induced retinal degeneration in rats. Neurosci Lett 367(2):205–209.

Chen S, Nguyen N, Tamura K, Karin M, Tukey RH. 2003. The role of the Ah receptor and p38 in benzo[a]pyrene-7,8-dihydrodiol and benzo[a]pyrene-7,8-dihydrodiol-9,10-epoxide-induced apoptosis. J Biol Chem 278(21):19526–19533.

Chin BY, Choi ME, Burdick MD, Strieter RM, Risby TH, Choi AM. 1998. Induction of apoptosis by particulate matter: Role of TNF-alpha and MAPK. Am J Physiol 275(5 Pt 1):L942–L949.

Chipuk JE, Bouchier-Hayes L, Kuwana T, Newmeyer DD, Green DR. 2005. PUMA couples the nuclear and cytoplasmic proapoptotic function of p53. Science 309(5741):1732–1735.

Dertinger SD, Lantum HB, Silverstone AE, Gasiewicz TA. 2000. Effect of 3′-methoxy-4′-nitroflavone on benzo[a]pyrene toxicity. Aryl hydrocarbon receptor-dependent and -independent mechanisms. Biochem Pharmacol 60(2):189–196.

Gilot D, Loyer P, Corlu A, Glaise D, Lagadic-Gossmann D, Atfi A, Morel F, Ichijo H, Guguen-Guillouzo C. 2002. Liver protection from apoptosis requires both blockage of initiator caspase activities and inhibition of ASK1/JNK pathway via glutathione S-transferase regulation. J Biol Chem 277(51):49220–49229.

Hirpara JL, Clement MV, Pervaiz S. 2001. Intracellular acidification triggered by mitochondrial-derived hydrogen peroxide is an effector mechanism for drug-induced apoptosis in tumor cells. J Biol Chem 276(1):514–521.

Huc L, Gilot D, Gardyn C, Rissel M, Dimanche-Boitrel MT, Guillouzo A, Fardel O, Lagadic-Gossmann D. 2003. Apoptotic mitochondrial dysfunction induced by benzo(a)pyrene in liver epithelial cells: Role of p53 and pHi changes. Ann N Y Acad Sci 1010:167–170.

Huc L, Sparfel L, Rissel M, Dimanche-Boitrel MT, Guillouzo A, Fardel O, Lagadic-Gossmann D. 2004. Identification of Na^+/H^+ exchange as a new target for toxic polycyclic aromatic hydrocarbons. FASEB J 18(2):344–346.

Jeffers JR, Parganas E, Lee Y, Yang C, Wang J, Brennan J, MacLean KH, Han J, Chittenden T, Ihle JN, McKinnon PJ, Cleveland JL, Zambetti GP. 2003. Puma is an essential mediator of p53-dependent and -independent apoptotic pathways. Cancer Cell 4(4):321–328.

Joannard F, Rissel M, Gilot D, Anderson A, Orfila-Lefeuvre L, Guillouzo A, Atfi A, Lagadic-Gossmann D. 2006. Role for mitogen-activated protein kinases in phenobarbital-induced expression of cytochrome P450 2B in primary cultures of rat hepatocytes. Toxicol Lett 161(1):61–72.

Khaled AR, Reynolds DA, Young HA, Thompson CB, Muegge K, Durum SK. 2001. Interleukin-3 withdrawal induces an early increase in mitochondrial membrane potential unrelated to the Bcl-2 family. Roles of intracellular pH, ADP transport, and F(0)F(1)-ATPase. J Biol Chem 276(9):6453–6462.

Knight RA, Petit PX. 2001. Another genotoxic agent released by mitochondrial meltdown. Cell Death Differ 8(12):1134–1135.

Kwon YW, Ueda S, Ueno M, Yodoi J, Masutani H. 2002. Mechanism of p53-dependent apoptosis induced by 3-methylcholanthrene: Involvement of p53 phosphorylation and p38 MAPK. J Biol Chem 277(3):1837–1844.

Lagadic-Gossmann D, Huc L, Lecureur V. 2004. Alterations of intracellular pH homeostasis in apoptosis: Origins and roles. Cell Death Differ 11(9):953–961.
Lang F, Madlung J, Bock J, Lukewille U, Kaltenbach S, Lang KS, Belka C, Wagner CA, Lang HJ, Gulbins E, Lepple-Wienhues A. 2000. Inhibition of Jurkat-T-lymphocyte Na^+/H^+-exchanger by CD95(Fas/Apo-1)-receptor stimulation. Pflugers Arch 440(6):902–907.
Lemarie A, Lagadic-Gossmann D, Morzadec C, Allain N, Fardel O, Vernhet L. 2004. Cadmium induces caspase-independent apoptosis in liver Hep3B cells: Role for calcium in signaling oxidative stress-related impairment of mitochondria and relocation of endonuclease G and apoptosis-inducing factor. Free Radic Biol Med 36(12):1517–1531.
Matikainen T, Perez GI, Jurisicova A, Pru JK, Schlezinger JJ, Ryu HY, Laine J, Sakai T, Korsmeyer SJ, Casper RF, Sherr DH, Tilly JL. 2001. Aromatic hydrocarbon receptor-driven Bax gene expression is required for premature ovarian failure caused by biohazardous environmental chemicals. Nat Genet 28(4):355–360.
Matsuyama S, Reed JC. 2000. Mitochondria-dependent apoptosis and cellular pH regulation. Cell Death Differ 7(12):1155–1165.
Matsuyama S, Xu Q, Velours J, Reed JC. 1998. The Mitochondrial F0F1-ATPase proton pump is required for function of the proapoptotic protein Bax in yeast and mammalian cells. Mol Cell 1(3):327–336.
Matsuyama S, Llopis J, Deveraux QL, Tsien RY, Reed JC. 2000. Changes in intramitochondrial and cytosolic pH: Early events that modulate caspase activation during apoptosis. Nat Cell Biol 2(6):318–325.
Michels J, Johnson PW, Packham G. 2005. Mcl-1. Int J Biochem Cell Biol 37(2):267–271.
Mort JS, Buttle DJ. 1997. Cathepsin B. Int J Biochem Cell Biol 29(5):715–720.
Nakano K, Vousden KH. 2001. PUMA, a novel proapoptotic gene, is induced by p53. Mol Cell 7(3):683–694.
Nebert DW, Dalton TP, Okey AB, Gonzalez FJ. 2004. Role of aryl hydrocarbon receptor-mediated induction of the CYP1 enzymes in environmental toxicity and cancer. J Biol Chem 279(23):23847–23850.
Norbury CJ, Zhivotovsky B. 2004. DNA damage-induced apoptosis. Oncogene 23(16):2797–2808.
Payen L, Courtois A, Langouet S, Guillouzo A, Fardel O. 2001. Unaltered expression of multidrug resistance transporters in polycyclic aromatic hydrocarbon-resistant rat liver cells. Toxicology 156(2–3):109–117.
Pelkonen O, Nebert DW. 1982. Metabolism of polycyclic aromatic hydrocarbons: Etiologic role in carcinogenesis. Pharmacol Rev 34(2):189–222.
Pfeifer GP, Denissenko MF, Olivier M, Tretyakova N, Hecht SS, Hainaut P. 2002. Tobacco smoke carcinogens, DNA damage and p53 mutations in smoking-associated cancers. Oncogene 21(48):7435–7451.
Poppe M, Reimertz C, Dussmann H, Krohn AJ, Luetjens CM, Bockelmann D, Nieminen AL, Kogel D, Prehn JH. 2001. Dissipation of potassium and proton gradients inhibits mitochondrial hyperpolarization and cytochrome c release during neural apoptosis. J Neurosci 21(13):4551–4563.
Roy S, Bayly CI, Gareau Y, Houtzager VM, Kargman S, Keen SL, Rowland K, Seiden IM, Thornberry NA, Nicholson DW. 2001. Maintenance of caspase-3 proenzyme dormancy by an intrinsic "safety catch" regulatory tripeptide. Proc Natl Acad Sci USA 98(11):6132–6137.
Salazar I, Pavani M, Aranda W, Maya JD, Morello A, Ferreira J. 2004. Alterations of rat liver mitochondrial oxidative phosphorylation and calcium uptake by benzo[a]pyrene. Toxicol Appl Pharmacol 198(1):1–10.
Schafer P, Scholz SR, Gimadutdinow O, Cymerman IA, Bujnicki JM, Ruiz-Carrillo A, Pingoud A, Meiss G. 2004. Structural and functional characterization of mitochondrial EndoG, a sugar non-specific nuclease which plays an important role during apoptosis. J Mol Biol 338(2):217–228.
Schneiderhan N, Budde A, Zhang Y, Brune B. 2003. Nitric oxide induces phosphorylation of p53 and impairs nuclear export. Oncogene 22(19):2857–2868.
Solhaug A, Refsnes M, Lag M, Schwarze PE, Husoy T, Holme JA. 2004. Polycyclic aromatic hydrocarbons induce both apoptotic and anti-apoptotic signals in Hepa1c1c7 cells. Carcinogenesis 25(5):809–819.
Sparfel L, Huc L, Le Vee M, Desille M, Lagadic-Gossmann D, Fardel O. 2004. Inhibition of carcinogen-bioactivating cytochrome P450 1 isoforms by amiloride derivatives. Biochem Pharmacol 67(9):1711–1719.
Tithof PK, Elgayyar M, Cho Y, Guan W, Fisher AB, Peters-Golden M. 2002. Polycyclic aromatic hydrocarbons present in cigarette smoke cause endothelial cell apoptosis by a phospholipase A2-dependent mechanism. FASEB J 16(11):1463–1464.
Torriglia A, Perani P, Brossas JY, Chaudun E, Treton J, Courtois Y, Counis MF. 1998. L-DNase II, a molecule that links proteases and endonucleases in apoptosis, derives from the ubiquitous serpin leukocyte elastase inhibitor. Mol Cell Biol 18(6):3612–3619.
Weng C, Li Y, Xu D, Shi Y, Tang H. 2005. Specific cleavage of Mcl-1 by caspase-3 in tumor necrosis factor-related apoptosis-inducing ligand (TRAIL)-induced apoptosis in Jurkat leukemia T cells. J Biol Chem 280(11):10491–10500.
Wenzel A, Grimm C, Samardzija M, Reme CE. 2005. Molecular mechanisms of light-induced photoreceptor apoptosis and neuroprotection for retinal degeneration. Prog Retin Eye Res 24(2):275–306.
Yu J, Zhang L, Hwang PM, Kinzler KW, Vogelstein B. 2001. PUMA induces the rapid apoptosis of colorectal cancer cells. Mol Cell 7(3):673–682.
Zamzami N, Kroemer G. 2001. The mitochondrion in apoptosis: How Pandora's box opens. Nat Rev Mol Cell Biol 2(1):67–71.